Kinetic aspects of discrete Cosserat rods based on the difference geometry of framed curves

Joachim Linn[1], Tomas Hermansson[2], Fredrik Andersson[2], Fabio Schneider[1]

[1] Fraunhofer ITWM
Fraunhofer–Platz 1, 67663 Kaiserslautern, Germany
[joachim.linn, fabio.schneider]@itwm.fraunhofer.de

[2] Fraunhofer–Chalmers Centre FCC
Chalmers Science Park, SE-412 88, Gothenburg, Sweden
[tomas.hermansson, fredrik.andersson]@fcc.chalmers.se

Abstract

The theory of *Cosserat rods* provides a self consistent framework for modeling large spatial deformations of slender flexible structures at small local strains. Discrete Cosserat rod models [1, 2] based on geometric finite differences preserve essential properties of the continuum theory. The present work investigates kinetic aspects of discrete quaternionic Cosserat rods defined on a staggered grid within the framework of Lagrangian mechanics. Assuming hyperelastic constitutive behaviour, the Euler–Lagrange equations of the model are shown to be equivalent to the (semi)discrete balance equations of forces, moments and inertial terms obtained from a direct discretization of the continuous balance equations via spatial finite differences along the centerline curve. Therefore, equilibrium configurations obtained by energy minimization correspond to solutions of the quasi-static balance equations. We illustrate this approach by two academic examples (Euler's *Elastica* and Kirchhoff's *helix*) and highlight its utility for practical applications with a use case from automotive industry (analysis of the layout of cooling hoses in the engine compartment of a passenger car).

Keywords: Cosserat rods, discrete balance equations, geometric finite differences, Lagrangian mechanics

1. Introduction

The theory of *Cosserat rods* [3, 4, 5] provides a self consistent framework for modeling large spatial deformations of slender flexible structures at small local strains. The main deformation modes of a Cosserat rod are *bending* and *twisting*, accompanied by very small, but in general non-zero amounts of longitudinal *stretching* (or compression), and *transverse shearing*, related to tiny out-of-plane cross section deformations. Discrete Cosserat rod models may be derived in terms of a finite difference approximation that preserves essential geometric properties of the continuum theory [6, 1, 2]. In a recent contribution [7], we discussed the *discrete kinematics* of Cosserat rods, based on the difference geometry of framed space curves defined on a staggered grid (see Fig. 1). The present work complements these considerations, with a focus on *kinetic* aspects.
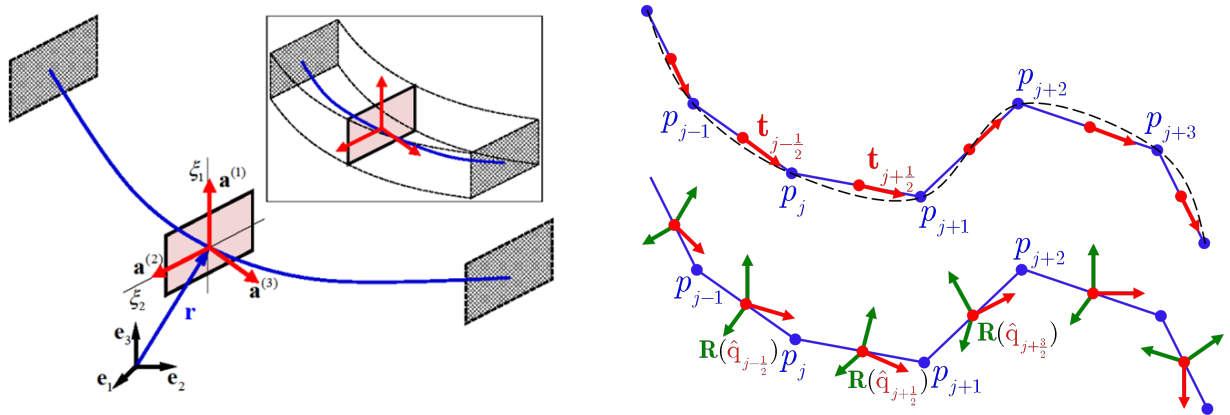

Figure 1: *Left:* Centerline curve $\mathbf{r}(s)$ and attached moving frame $\mathsf{R}(s) = \mathbf{a}^{(k)}(s) \otimes \mathbf{e}_k$ of a *Cosserat curve*, describing the geometry of the configurations of a prismatic rod in Euclidian space. The volumetric geometry is generated by sliding the cross section spanned by the frame directors $\{\mathbf{a}^{(1)}, \mathbf{a}^{(2)}\}$ along the centerline. The position vectors of the material points in the rod volume are parametrized by: $\mathbf{x} = \mathbf{r}(s) + \xi_\alpha \mathbf{a}^{(\alpha)}(s)$. *Right:* Polygonal arc approximating a smooth regular geometric curve $\mathscr{C}$: The vertices $p_j \in \mathscr{C}$ located at positions $\mathbf{r}_j \in \mathbb{E}^3$ define edges $[p_{j-1}, p_j]$ of length $\ell_{j-1/2}$, with edge centered unit length tangent vectors $\mathbf{t}_{j-1/2}$. A *discrete Cosserat curve* [7] consists of a polygonal arc with edge centered quaternions $\hat{\mathsf{q}}_{j-1/2} \in S^3$, representing frames $\mathsf{R}_{j-1/2} = \mathfrak{E}(\hat{\mathsf{q}}_{j-1/2})$ via the *Euler map* $\mathfrak{E} : S^3 \to \mathsf{SO}(3)$.

As sketched on the left of Fig. 1, the kinematic skeleton of a Cosserat rod configuration corresponds to a *framed curve* (or *Cosserat curve*), parametrized by the arc length s of its centerline $\mathbf{r}(s)$, augmented by a moving quaternion frame field $\hat{\mathsf{q}}(s) \in S^3$. The material curvature and tangent vector fields $\mathbf{K} = 2\hat{\mathsf{q}}^* \circ \partial_s \hat{\mathsf{q}}$ and $\boldsymbol{\Gamma} = \hat{\mathsf{q}}^* \circ \partial_s \mathbf{r} \circ \hat{\mathsf{q}}$ are the *differential invariants* that determine the geometry of a Cosserat curve uniquely, up to a global rigid body motion. In the case of *dynamic* motions, the *velocity* $\mathbf{v} = \partial_t \mathbf{r}$ of points on the centerline and the *angular velocity* $\boldsymbol{\omega} = 2\partial_t \hat{\mathsf{q}} \circ \hat{\mathsf{q}}^*$ of the local cross section rotations w.r.t. the global inertial frame, or equivalently its material counterpart given by $\boldsymbol{\Omega} = \hat{\mathsf{q}}^* \circ \boldsymbol{\omega} \circ \hat{\mathsf{q}} = 2\hat{\mathsf{q}}^* \circ \partial_t \hat{\mathsf{q}}$ and subject to the *compatibility* condition $\partial_s \boldsymbol{\Omega} - \partial_t \mathbf{K} \equiv \mathbf{K} \times \boldsymbol{\Omega}$, are additional kinematical variables that characterize the space–time configuration of a Cosserat rod. Local *strains* occurring in Cosserat rod configurations, deformed w.r.t. a given reference state, are described in terms of the difference functions $\Delta \mathbf{K}(s,t) \equiv \mathbf{K}(s,t) - \mathbf{K}_0(s)$ and $\Delta \boldsymbol{\Gamma}(s,t) \equiv \boldsymbol{\Gamma}(s,t) - \boldsymbol{\Gamma}_0$ measuring the deviations of the invariants from their reference values $\mathbf{K}_0(s)$ and $\boldsymbol{\Gamma}_0 = \mathbf{e}_3$.

The basic *kinetic* quantities of a Cosserat rod are the sectional force $\mathbf{f}(s,t)$, also denoted as *stress resultant*, and the sectional moment $\mathbf{m}(s,t)$, also denoted as *stress couple*. Both vector fields are *spatial* quantities obtained by the integration of traction forces over the local cross section area, and respectively the integrated couples resulting from these traction forces w.r.t. the cross section center. The kinetic sectional quantitites are both functions of the curve parameter s, usually chosen as the *arc length* of the centerline in its reference configuration, and the *time t*. Their dynamic equilibrium is governed by the *balance equations for linear and angular momentum*

$$\partial_s \mathbf{f} + \boldsymbol{\beta} \;=\; \rho_L \, \partial_t \mathbf{v} \;, \quad \partial_s \mathbf{m} + \partial_s \mathbf{r} \times \mathbf{f} + \boldsymbol{\mu} \;=\; \partial_t \left([\rho_L \mathsf{J}] \cdot \boldsymbol{\omega} \right) \;. \tag{1}$$

The inertial terms on the r.h.s. are the time derivatives of the translational momentum density $\rho_L \mathbf{v}$ of infinitesimal mass segments with density ρ_L on the centerline of the rod, and the angular momentum density $[\rho_L \mathsf{J}] \cdot \boldsymbol{\omega}$ of the corresponding cross sections, proportional to their rotational inertia tensor $[\rho_L \mathsf{J}]$ w.r.t. the global inertial frame.

Consistent with the staggered discretization approach for Cosserat rods [2], *semi-discrete balance equations* may be formally derived from the continuous ones by integrating the equations (1) over parameter intervals between adjacent edge centers $s_{j\pm1/2}$ around a vertex $\mathbf{r}_j = \mathbf{r}(s_j)$, and over intervals between adjacent vertices. With an approximation of integral terms by midpoint quadrature one obtains the semi-discrete system of equations

$$\mathbf{f}_{j+1/2} - \mathbf{f}_{j-1/2} + \bar{h}_j \boldsymbol{\beta}_j \;=\; \bar{h}_j \rho_L \partial_t \mathbf{v}_j \,, \tag{2}$$

$$\mathbf{m}_{j+1} - \mathbf{m}_j + (\mathbf{r}_{j+1} - \mathbf{r}_j) \times \mathbf{f}_{j+1/2} + h_{j+1/2} \boldsymbol{\mu}_{j+1/2} \;=\; h_{j+1/2} \partial_t \left([\rho_L \mathsf{J}]_{j+1/2} \cdot \boldsymbol{\omega}_{j+1/2} \right) \,, \tag{3}$$

where $\boldsymbol{\beta}_j$ and $\boldsymbol{\mu}_{j+1/2}$ denote the integral averages of the external force and moment vector fields $\boldsymbol{\beta}$ and $\boldsymbol{\mu}$ over the respective intervals of lengths $\bar{h}_j := \frac{1}{2}(h_{j-1/2} + h_{j-1/2}) = \frac{1}{2}(s_{j+1/2} - s_{j-1/2})$ and $h_{j+1/2} := s_{j+1} - s_j$.

While this semi-discrete system provides a consistent *finite difference discretization* of the continuous balance equations (1) displaying obvious formal similarities, it is less obvious that a semi-discrete system of this form results as an equivalent of the *Euler–Lagrange equations* of our discrete quaternionic Cosserat rod model, if a hyperelastic constitutive behaviour of the rod material is assumed. In this case the semi-discrete force and moment vectors $\mathbf{f}_{j+1/2}(t)$ and $\mathbf{m}_j(t)$ defined at the edge centers and the vertices of the staggered grid are given as gradients of a *stored energy* potential function $\mathscr{W}^{(el)}(\{\boldsymbol{\Gamma}_{j-1/2}\}_{j=1,\dots,N}, \{\mathbf{K}_j\}_{j=0,\dots,N})$ w.r.t. the discrete material shear–extensional strain vectors given by $\boldsymbol{\Gamma}_{j+1/2} := \hat{\mathsf{q}}^*_{j+1/2} \circ (\mathbf{r}_{j+1} - \mathbf{r}_j)/h_{j+1/2} \circ \hat{\mathsf{q}}_{j+1/2}$, and material curvature vectors $\mathbf{K}_j := 2\log(\hat{\mathsf{q}}^*_{j-1/2} \circ \hat{\mathsf{q}}_{j+1/2})/\bar{h}_j$ extracted from the difference rotations connecting adjacent frames $\hat{\mathsf{q}}_{j\pm1/2}$, both rotated to the global inertial frame according to:

$$\mathbf{f}_{j+1/2} \;=\; \hat{\mathsf{q}}_{j+1/2} \circ \frac{\partial \mathscr{W}^{(el)}}{\partial \boldsymbol{\Gamma}_{j+1/2}} \circ \hat{\mathsf{q}}^*_{j+1/2} \;=\; \mathsf{R}_{j+1/2} \cdot \mathbf{F}_{j+1/2} \;, \quad \mathbf{m}_j \;=\; \hat{\mathsf{q}}_{j+1/2} \circ \frac{\partial \mathscr{W}^{(el)}}{\partial \mathbf{K}_j} \circ \hat{\mathsf{q}}^*_{j+1/2} \;=\; \mathsf{R}_{j+1/2} \cdot \mathbf{M}_j \;. \tag{4}$$

While a derivation of the semi-discrete balance equations (2) of the sectional forces is straightforward, it is less obvious that the semi-discrete balance equations of the sectional momenta as given in [2] in quaternionic form are equivalent to equations of the form (3).

In our contribution, we investigate these issues and thereby elucidate the kinetic aspects of our discrete Cosserat rod model. We also present applications of our Lagrangian approach to discrete Cosserat rod models in computing equilibrium configurations of elastic cables by minimizing their potential energy w.r.t. given boundary conditions. We investigate some properties of this approach by a discussion of two well known, analytically solvable test examples: The bending of an *Elastica* in the plane, and the bending and twisting of a straight rod to a *helix* in space. Moreover, we point out applications in automotive industry, illustrated by a typical use case: The analysis of the layout of cooler hoses in the engine compartment of a passenger car.

2. Langrangian mechanics of Cosserat rods

Assuming a hyperelastic constitutive behaviour, the dynamic balance equations of a Cosserat rod can be derived according to *Hamilton's principle*[1] of stationary action, which states that the variational derivative of the *Lagrangian density* $\mathscr{L} = \mathscr{T} - \mathscr{V}$ of the rod, vanishes identically for configurations in mechanical equilibrium, such that the *Euler–Lagrange equations* $\partial_t \left(\nabla_{\partial_t \boldsymbol{\chi}} \mathscr{L} \right) = \nabla_{\boldsymbol{\chi}} \mathscr{L} - \partial_s \left(\nabla_{\partial_s \boldsymbol{\chi}} \mathscr{L} \right)$ are satisfied. The Lagrangian density $\mathscr{L}$ depends on the field of configuration variables $\boldsymbol{\chi}(s,t) := (\mathbf{r}(s,t), \hat{q}(s,t)) \in \mathbb{E}^3 \times S^3$ of the rod, and on their partial space and time derivatives $\partial_s \boldsymbol{\chi} = (\partial_s \mathbf{r}, \partial_s \hat{q})$ and $\partial_t \boldsymbol{\chi} = (\partial_t \mathbf{r}, \partial_t \hat{q})$, respectively.

2.1. Kinetic and stored energy densities of Cosserat rods

The kinetic energy of a Cosserat rod is given by the integral $W^{(kin)} = \int_0^L ds\, \mathscr{T}$ of the corresponding *kinetic energy density* $\mathscr{T} = \frac{1}{2}\rho_L \mathbf{v}^2 + \frac{1}{2}\langle \boldsymbol{\Omega}^T, [\rho I_0] \cdot \boldsymbol{\Omega} \rangle$. The inertial properties of the rod are described by the *mass per length* $\rho_L(s)$ and the cross sectional *inertia tensor* $[\rho I_0](s)$ w.r.t. the material frame. In the case of a prismatic rod with constant cross section area A, constant area moments $I_{1,2}$ and J and a homogeneous volumetric mass density ρ_0, the inertial parameters are simply given by $\rho_L = \rho_0 A$ and $[\rho I_0] = \rho_0 \operatorname{diag}(I_1, I_2, J)$.

In the absence of external forces and moments acting on the rod, the potential energy of the rod is given by its *stored energy* functional $W^{(el)} = \int_0^L ds\, \mathscr{V}^{(el)}(\boldsymbol{\Gamma}, \mathbf{K})$. Frame invariance implies that its density function $\mathscr{V}^{(el)}$ may depend on the configuration variables $(\mathbf{r}, \hat{q})$ and their spatial derivatives $(\partial_s \mathbf{r}, \partial_s \hat{q})$ only via the invariants $\boldsymbol{\Gamma}$ and $\mathbf{K}$. Hyperelastic constitutive equations for a Cosserat rod are then given by the relations $\mathbf{F} = \partial \mathscr{V}^{(el)}/\partial \boldsymbol{\Gamma}$ and $\mathbf{M} = \partial \mathscr{V}^{(el)}/\partial \mathbf{K}$ providing the material kinetic quantities $\mathbf{F}$ and $\mathbf{M}$ in terms of derivatives of the stored energy density w.r.t. the invariants, with corresponding spatial force and moment vectors resulting from a push forward rotation of the global basis to the local frame of the deformed configuration according to $\mathbf{f} = \hat{q} \circ \mathbf{F} \circ \hat{q}^*$ and $\mathbf{m} = \hat{q} \circ \mathbf{M} \circ \hat{q}^*$.

In the simplest and most frequently considered case, the elastic energy density is given by a diagonal quadratic form $\mathscr{V}^{(el)}(\boldsymbol{\Gamma}, \mathbf{K}) = \frac{1}{2}\langle \Delta\boldsymbol{\Gamma}, \mathsf{C}_\Gamma \cdot \Delta\boldsymbol{\Gamma} \rangle + \frac{1}{2}\langle \Delta\mathbf{K}, \mathsf{C}_K \cdot \Delta\mathbf{K} \rangle$, characterized by the *effective stiffness parameters* of the local cross section assembled in the diagonal matrices $\mathsf{C}_\Gamma = \operatorname{diag}([GA_1], [GA_2], [EA])$ and $\mathsf{C}_K = \operatorname{diag}([EI_1], [EI_2], [GJ])$, which may be variable along the rod, but often are assumed to be constant. More general, the local effective stiffness properties may be modeled by symmetric matrices C_Γ and C_K, containing off-diagonal coupling terms. In all cases, the constitutive equations are given by the linear relations $\mathbf{F} = \mathsf{C}_\Gamma \cdot \Delta\boldsymbol{\Gamma}$, $\mathbf{M} = \mathsf{C}_K \cdot \Delta\mathbf{K}$.

In some more advanced applications of Cosserat rod models, cross-coupling of forces and moments appear, e.g. in the case of ropes, where longitudinal tension may induce a torsional torque, or in the case of rotor blades where the shear and geometrical centers of the cross section do in general not coincide, such that the transverse shear force and torsional moment become coupled [8]. To simplify the development of our discrete Cosserat model variant we do not consider such cross-coupling terms by assuming that second order mixed partial derivatives of the stored energy density w.r.t. the invariants vanish, such that $\partial \mathbf{F}/\partial \mathbf{K} = 0 = \partial \mathbf{M}/\partial \boldsymbol{\Gamma}$ holds. This motivates an additive decomposition ansatz for the stored energy density according to $\mathscr{V}^{(el)}(\boldsymbol{\Gamma}, \mathbf{K}) = \mathscr{V}_{\mathbf{F}}^{(el)}(\boldsymbol{\Gamma}) + \mathscr{V}_{\mathbf{M}}^{(el)}(\mathbf{K})$.

2.2. Potential density functions for external forces and moments

External forces $\boldsymbol{\beta}$ and moments $\boldsymbol{\mu}$ may be incorporated into the Lagrangian formalism by assuming that both vector quantities can likewise be derived from potential energy density terms as gradients w.r.t. the configuration variables.

A simple example is a dead load given by the potential density function $\mathscr{V}_{\boldsymbol{\beta}}^{(ext)} = -\langle \mathbf{r}, \boldsymbol{\beta} \rangle$, which yields the external force $\boldsymbol{\beta} = -\partial \mathscr{V}_{\boldsymbol{\beta}}^{(ext)}/\partial \mathbf{r}$. The latter relation holds likewise for more complicated potential functions. The gravitational force per unit length acting on a rod is $\boldsymbol{\beta} = -\rho_L g_0 \mathbf{e}_3$, proportional to the mass per length ρ_L and $g_0 = 9.81\, m/s^2$.

The treatment of external moments derived from a potential is technically more involved, due to gradient terms w.r.t. moving frames, which are variables on a manifold. Following Antman's considerations, the *rotational gradient* may be formulated in terms of the frame directors as $\boldsymbol{\mu} = -\mathbf{a}^{(k)} \times \partial \mathscr{V}_{\boldsymbol{\mu}}^{(ext)}/\partial \mathbf{a}^{(k)} \equiv -\nabla_R \mathscr{V}_{\boldsymbol{\mu}}^{(ext)}$, where the latter expressions symbolizes the gradient operation w.r.t. $SO(3)$ frames. As a concrete example, we consider a dead load given by a body force field $\mathbf{b}(\mathbf{x})$ acting at the positions $\mathbf{x} = \mathbf{r}(s) + \xi_\alpha \mathbf{a}^{(\alpha)}(s)$ of the material points of an arbitrary deformed configuration of a Cosserat rod body (see Fig. 1). In the three-dimensional theory, the corresponding potential energy is given by the integral $-\int_0^L ds \int_A dA\, \langle \mathbf{x}, \mathbf{b} \rangle = \int_0^L ds\, \left[\mathscr{V}_{\boldsymbol{\beta}}^{(ext)} + \mathscr{V}_{\boldsymbol{\mu}}^{(ext)} \right]$, with $\mathscr{V}_{\boldsymbol{\beta}}^{(ext)} = -\langle \mathbf{r}, \boldsymbol{\beta} \rangle$, where $\boldsymbol{\beta} = \int_A dA\, \mathbf{b}$ equals the net force acting on the centerline points $\mathbf{r}(s)$. The potential for the external moments is given by $\mathscr{V}_{\boldsymbol{\mu}}^{(ext)} = -\int_A dA\, \langle \boldsymbol{\xi}, \mathbf{b} \rangle$, with $\boldsymbol{\xi} = \xi_\alpha \mathbf{a}^{(\alpha)}$ pointing to the positions of points in the cross section w.r.t. its center.

---

[1]For a detailed exposition of the mathematical problem we refer to section 16. in Ch. 8 of Antman's book [3].

This yields $\boldsymbol{\mu} = -\nabla_{\mathsf{R}} \mathscr{V}_{\boldsymbol{\mu}}^{(ext)} = \int_A dA\,\boldsymbol{\xi} \times \mathbf{b}$, which corresponds to the integrated torques generated by the body force field w.r.t. the centerline position. In the case of gravity, the body force is given by $\mathbf{b}(\mathbf{x}) = -\rho(\mathbf{x})g_0\mathbf{e}_3$, which yields $\boldsymbol{\beta}(s) = -\rho_L(s)g_0\mathbf{e}_3$ with $\rho_L(s) = \int_A dA\,\rho(\mathbf{x})$. If the mass density is constant, the geometrical center of the cross section coincides with its center of gravity, such that the corresponding moment $\boldsymbol{\mu}$ vanishes. This also holds in the case of symmetric cross section shapes and a likewise symmetric mass distribution within the cross section.

The *Euler map* $S^3 \ni \hat{\mathsf{q}} \mapsto \mathfrak{E}(\hat{\mathsf{q}}) = \mathsf{R} \in SO(3)$ is implicitly defined by its action on vectors $\mathbf{u} \in \mathbb{E}^3$ as: $\mathfrak{E}(\hat{\mathsf{q}}) \cdot \mathbf{u} = \hat{\mathsf{q}} \circ \mathbf{u} \circ \hat{\mathsf{q}}^*$. A quaternionic formulation of $\mathscr{V}_{\boldsymbol{\mu}}^{(ext)}$ can be derived from the parametrization of $SO(3)$ frames by rotational quaternions via the Euler map $\mathsf{R} = \mathfrak{E}(\hat{\mathsf{q}})$ and the implied representation $\mathbf{a}^{(k)} = \mathfrak{E}(\hat{\mathsf{q}}) \cdot \mathbf{e}_k$ of the frame directors. For the quaternionic potential defined as $\hat{\mathscr{V}}_{\boldsymbol{\mu}}^{(ext)}(\hat{\mathsf{q}}) := \mathscr{V}_{\boldsymbol{\mu}}^{(ext)}(\mathfrak{E}(\hat{\mathsf{q}}))$, the quaternionic equivalent $\nabla_{\hat{\mathsf{q}}}$ of ∇_{R} can be defined in terms of the partial derivatives $\partial/\partial\mathbf{a}^{(k)} \equiv [d\mathfrak{E}(\hat{\mathsf{q}}) \cdot \mathbf{e}_k]^{-T} \cdot \partial/\partial\hat{\mathsf{q}}$ using the inverse transpose of the derivative $d\mathfrak{E} : TS^3 \to TSO(3)$ of the Euler map, resulting in: $\nabla_{\mathsf{R}}\mathscr{V}_{\boldsymbol{\mu}}^{(ext)}(\mathsf{R}) \equiv \nabla_{\hat{\mathsf{q}}}\hat{\mathscr{V}}_{\boldsymbol{\mu}}^{(ext)}(\hat{\mathsf{q}}) := (\mathfrak{E}(\hat{\mathsf{q}}) \cdot \mathbf{e}_k) \times [d\mathfrak{E}(\hat{\mathsf{q}}) \cdot \mathbf{e}_k]^{-T} \cdot \partial\hat{\mathscr{V}}_{\boldsymbol{\mu}}^{(ext)}(\hat{\mathsf{q}})/\partial\hat{\mathsf{q}}$.

2.3. The Lagrangian of a discrete Cosserat rod

The *Lagrangian function* of a discrete Cosserat rod may be obtained by a discretization of the integral $\int_0^L ds\,\mathscr{L}$, as discussed in detail in [2]. Here we present a version of the semi-discrete model that is more general w.r.t. the assumptions of the stored energy, but we omit viscous damping effects [9].

The *total potential energy* $W^{(pot)} = W^{(el)} + W^{(ext)}$ consists of the sum of the *stored energy* functional $W^{(el)} = \int_0^L ds\,\mathscr{V}^{(el)}$ with the *stored energy density* $\mathscr{V}^{(el)}(\boldsymbol{\Gamma},\mathbf{K}) = \mathscr{V}_{\mathbf{F}}^{(el)}(\boldsymbol{\Gamma}) + \mathscr{V}_{\mathbf{M}}^{(el)}(\mathbf{K})$ and the potential $W^{(ext)} = \int_0^L ds\left[\mathscr{V}_{\boldsymbol{\beta}}^{(ext)} + \hat{\mathscr{V}}_{\boldsymbol{\mu}}^{(ext)}\right]$ from which the external forces and moments are obtained as gradients of the densities $\mathscr{V}_{\boldsymbol{\beta}}^{(ext)}(\mathbf{r})$ and $\hat{\mathscr{V}}_{\boldsymbol{\mu}}^{(ext)}(\hat{\mathsf{q}})$.

The discretization scheme of the *Lagrangian* $\int_0^L ds\,\mathscr{L}$ is induced by the *discrete kinematics* [7, 10] of a Cosserat rod. In the discrete model sketched in Fig. 1 on the right, *discrete material curvatures* $\mathbf{K}_j := 2\log(\hat{\mathsf{q}}_{j-1/2}^* \circ \hat{\mathsf{q}}_{j+1/2})/\bar{h}_j$ are vertex based quantities extracted from the difference rotations connecting adjacent quaternion frames $\hat{\mathsf{q}}_{j\pm 1/2}$, while the *discrete material shear–extensional strain vectors* $\boldsymbol{\Gamma}_{j+1/2} := \hat{\mathsf{q}}_{j+1/2}^* \circ (\mathbf{r}_{j+1} - \mathbf{r}_j)/h_{j+1/2} \circ \hat{\mathsf{q}}_{j+1/2}$ are egde-centered quantities. The latter fact motivates an approximation $\int_{s_{j-1}}^{s_j} ds\,\mathscr{V}_{\mathbf{F}}^{(el)}(\boldsymbol{\Gamma}) \approx h_{j-1/2}\,\mathscr{V}_{\mathbf{F}}^{(el)}(\boldsymbol{\Gamma}_{j-1/2})$ on the subintervals $[s_{j-1},s_j]$ by the midpoint rule, which results in the discrete approximation

$$W_{\mathbf{F}}^{(el)} := \int_0^L ds\,\mathscr{V}_{\mathbf{F}}^{(el)}(\boldsymbol{\Gamma}) \approx \sum_{j=1}^N h_{j-1/2}\,\mathscr{V}_{\mathbf{F}}^{(el)}(\boldsymbol{\Gamma}_{j-1/2}) =: \mathscr{W}_{\mathbf{F}}^{(el)} \tag{5}$$

of the total stored energy part related to *extensional and transverse shear* deformations of the rod. The other part related to *bending and torsion* deformations is discretized by trapezoidal quadrature as

$$W_{\mathbf{M}}^{(el)} := \int_0^L ds\,\mathscr{V}_{\mathbf{M}}^{(el)}(\mathbf{K}) \approx \sum_{j=0}^N \bar{h}_j\,\mathscr{V}_{\mathbf{M}}^{(el)}(\mathbf{K}_j) =: \mathscr{W}_{\mathbf{M}}^{(el)}, \tag{6}$$

using the approximation $\int_{s_{j-1/2}}^{s_{j+1/2}} ds\,\mathscr{V}_{\mathbf{M}}^{(el)}(\mathbf{K}) \approx \bar{h}_j\,\mathscr{V}_{\mathbf{M}}^{(el)}(\mathbf{K}_j)$ of the partial integrals over subintervals between the interval midpoints $s_{j\pm 1/2} = \frac{1}{2}(s_j + s_{j\pm 1})$ around the inner vertices $j = 1,\ldots,N-1$, and analogously defined one sided approximations $\int_0^{s_{1/2}} ds\,\mathscr{V}_{\mathbf{M}}^{(el)}(\mathbf{K}) \approx \bar{h}_0\,\mathscr{V}_{\mathbf{M}}^{(el)}(\mathbf{K}_0)$ and $\int_{s_{N-1/2}}^{s_N} ds\,\mathscr{V}_{\mathbf{M}}^{(el)}(\mathbf{K}) \approx \bar{h}_N\,\mathscr{V}_{\mathbf{M}}^{(el)}(\mathbf{K}_N)$ at the intervals of halved lengths $\bar{h}_0 = \frac{1}{2}h_{1/2}$ and $\bar{h}_N = \frac{1}{2}h_{N-1/2}$ near the boundary vertices. Different from the curvatures $\mathbf{K}_j$ located at the inner vertices, the modified definitions $\mathbf{K}_0 := 2\log(\hat{\mathsf{q}}_0^* \circ \hat{\mathsf{q}}_{1/2})/\bar{h}_0$ and $\mathbf{K}_N := 2\log(\hat{\mathsf{q}}_{N-1/2}^* \circ \hat{\mathsf{q}}_N)/\bar{h}_N$ for the discrete boundary curvatures involve vertex based boundary frames $\hat{\mathsf{q}}_0$ and $\hat{\mathsf{q}}_N$ that appear in the discrete model due to boundary conditions, either explicitly, or by interpolation according to the *"shadow quaternion"* approach suggested in [2]. In summary, the sums given in (5) and (6) provide the desired discrete approximation $\mathscr{W}^{(el)} := \mathscr{W}_{\mathbf{F}}^{(el)} + \mathscr{W}_{\mathbf{M}}^{(el)} \approx W^{(el)} = \int_0^L ds\,\mathscr{V}^{(el)}$ of the *stored energy* functional of a Cosserat rod.

The discrete approximation $W^{(ext)} \approx \mathscr{W}^{(ext)} := \mathscr{W}_{\boldsymbol{\beta}}^{(ext)} + \hat{\mathscr{W}}_{\boldsymbol{\mu}}^{(ext)}$ of the external potential according to

$$\mathscr{W}_{\boldsymbol{\beta}}^{(ext)} := \sum_{j=0}^N \bar{h}_j\,\mathscr{V}_{\boldsymbol{\beta}}^{(ext)}(\mathbf{r}_j) \approx \int_0^L ds\,\mathscr{V}_{\boldsymbol{\beta}}^{(ext)}(\mathbf{r}) \ , \ \ \hat{\mathscr{W}}_{\boldsymbol{\mu}}^{(ext)} := \sum_{j=1}^N h_{j-1/2}\,\hat{\mathscr{V}}_{\boldsymbol{\mu}}^{(ext)}(\hat{\mathsf{q}}_{j-1/2}) \approx \int_0^L ds\,\hat{\mathscr{V}}_{\boldsymbol{\mu}}^{(ext)}(\hat{\mathsf{q}}) \ . \tag{7}$$

results analogously by approximating the respective partial integrals using trapezoidal and midpoint quadrature. This completes the definition of the *discrete potential energy* function $\mathscr{W}^{(pot)} := \mathscr{W}^{(el)} + \hat{\mathscr{W}}^{(ext)}$.

The discrete approximation of the *kinetic energy* $\mathscr{W}^{(kin)} := \mathscr{W}^{(tr)} + \mathscr{W}^{(rot)} \approx W^{(kin)}$ is obtained via the same scheme, with the discrete approximations

$$\mathscr{W}^{(tr)} := \frac{1}{2} \sum_{j=0}^{N} \bar{h}_j \rho_j \mathbf{v}_j^2 \approx \frac{1}{2} \int_0^L ds \, \rho_L \mathbf{v}^2 \,, \tag{8}$$

$$\mathscr{W}^{(rot)} := \frac{1}{2} \sum_{j=1}^{N} h_{j-1/2} \langle \mathbf{\Omega}_{j-1/2}^T, [\rho\mathsf{I}]_{j-1/2} \cdot \mathbf{\Omega}_{j-1/2} \rangle \approx \frac{1}{2} \int_0^L ds \, \langle \mathbf{\Omega}^T, [\rho\mathsf{I}_0] \cdot \mathbf{\Omega} \rangle \tag{9}$$

of the translational and rotational parts. According to (8), the vertices are equipped with *lumped masses* given by $\bar{h}_j \rho_j := \int_{s_{j-1/2}}^{s_{j+1/2}} ds \, \rho_l(s)$ and move with the velocity $\mathbf{v}_j(t) = \partial_t \mathbf{r}(s_j, t)$, and $h_{j-1/2} [\rho\mathsf{I}_0]_{j-1/2} := \int_{s_{j-1}}^{s_j} ds \, [\rho\mathsf{I}_0](s)$ is the constant *inertia tensor* of the segment $[p_{j-1}, p_j]$ w.r.t. the axes of the local frame $\hat{\mathsf{q}}_{j-1/2}(t)$, rotating with the *material angular velocity* $\mathbf{\Omega}_{j-1/2}(t) := \mathbf{\Omega}(s_{j-1/2}, t) = 2\hat{\mathsf{q}}_{j-1/2}^*(t) \circ \partial_t \hat{\mathsf{q}}_{j-1/2}(t)$. While the *boundary vertices* $\mathbf{r}_0$ and $\mathbf{r}_N$ have masses $\bar{h}_0 \rho_0$ and $\bar{h}_N \rho_N$, the *boundary frames* $\hat{\mathsf{q}}_0$ and $\hat{\mathsf{q}}_N$, which are utilized mainly for a proper formulation of boundary conditions, are *not* coupled to rotational inertia.

2.4. Semi-discrete balance equations

Having defined the *Lagrangian function* $\mathscr{L} = \mathscr{W}^{(kin)} - \mathscr{W}^{(pot)}$ of our semi-discrete Cosserat model, we may proceed to derive the *semi-discrete balance equations for linear and angular momentum* from *Hamilton's principle* of least (or stationary) action according to the formalism of Lagrangian mechanics.

The semi-discrete potential energy function $\mathscr{W}^{(pot)} = \mathscr{W}^{(el)} + \mathscr{W}^{(ext)}$ is a function of the vertices $\{\mathbf{r}_j\}_{j=0,\dots,N}$ and the quaternion frames $\{\hat{\mathsf{q}}_{j-1/2}\}_{j=1,\dots,N}$ defining the configuration of a discrete Cosserat rod. In accordance with frame invariance, the stored energy part $\mathscr{W}^{(el)} = \mathscr{W}_{\mathbf{F}}^{(el)} + \mathscr{W}_{\mathbf{M}}^{(el)}$ depends on the discrete configuration variables only via the discrete invariants $\{\mathbf{K}_j\}_{j=0,\dots,N}$ and $\{\mathbf{\Gamma}_{j-1/2}\}_{j=1,\dots,N}$. The discrete external potentials $\mathscr{W}_{\boldsymbol{\beta}}^{(ext)}$ and $\hat{\mathscr{W}}_{\boldsymbol{\mu}}^{(ext)}$ are assumed to have explicit dependence on the configuration variables. The semi-discrete kinetic energy $\mathscr{W}^{(kin)}$ is an invariant quadratic form of the vertex velocities $\{\mathbf{v}_j\}_{j=0,\dots,N}$ and the angular velocities $\{\mathbf{\Omega}_{j-1/2}\}_{j=1,\dots,N}$ of the edges.

The *semi-discrete Euler–Lagrange equations*[2] of our discrete Cosserat rod model are then formally given as follows:

$$\frac{\partial \bar{\mathscr{L}}}{\partial \mathbf{r}_j} = \partial_t \left(\frac{\partial \bar{\mathscr{L}}}{\partial \mathbf{v}_j} \right) \,, \quad \frac{\partial \bar{\mathscr{L}}}{\partial \hat{\mathsf{q}}_{j-1/2}} = \partial_t \left(\frac{\partial \bar{\mathscr{L}}}{\partial (\partial_t \hat{\mathsf{q}}_{j-1/2})} \right) \tag{10}$$

The first part related to the centerline positions and velocities $\mathbf{r}_j$ and $\mathbf{v}_j$ corresponds to the semi-discrete balance of momentum equations. Making use of (8), its r.h.s. directly yields $\bar{h}_j \rho_j \partial_t \mathbf{v}_j = \partial_t (\partial \mathscr{W}^{(tr)}/\partial \mathbf{v}_j) = \partial_t (\partial \mathscr{L}/\partial \mathbf{v}_j)$ and therefore results in the inertial terms on the r.h.s. of (2) for constant ρ_L. On the l.h.s. we need to evaluate $\partial \mathscr{L}/\partial \mathbf{r}_j = -\partial \mathscr{W}^{(pot)}/\partial \mathbf{r}_j = -\partial \mathscr{W}^{(el)}/\partial \mathbf{r}_j - \partial \mathscr{W}^{(ext)}/\partial \mathbf{r}_j$. The latter term results in $-\partial \mathscr{W}^{(ext)}/\partial \mathbf{r}_j = \bar{h}_j \boldsymbol{\beta}_j$, with the discrete external forces acting at the vertices given by $\boldsymbol{\beta}_j = -\partial \mathscr{V}_{\boldsymbol{\beta}}^{(ext)}/\partial \mathbf{r}_j$ according to (7). The stored energy function depends on the vertex positions $\mathbf{r}_j$ solely via the strains $\mathbf{\Gamma}_{j\pm1/2}$, such that $\partial \mathscr{W}^{(el)}/\partial \mathbf{r}_j = \partial \mathscr{W}_{\mathbf{F}}^{(el)}/\partial \mathbf{r}_j = h_{j-1/2} \partial \mathscr{V}_{\mathbf{F}}^{(el)}(\mathbf{\Gamma}_{j-1/2})/\partial \mathbf{r}_j + h_{j+1/2} \partial \mathscr{V}_{\mathbf{F}}^{(el)}(\mathbf{\Gamma}_{j+1/2})/\partial \mathbf{r}_j$ holds according to (5). The material sectional force vectors are given by $\mathbf{F}_{j\pm1/2} = \partial \mathscr{V}_{\mathbf{F}}^{(el)}/\partial \mathbf{\Gamma}_{j\pm1/2} = \partial \mathscr{W}^{(el)}/\partial \mathbf{\Gamma}_{j\pm1/2}$. Their spatial counterparts are obtained by a forward rotation of the material forces to the local frames, according to: $\mathbf{f}_{j\pm1/2} = \mathsf{R}_{j\pm1/2} \cdot \mathbf{F}_{j\pm1/2} \equiv \hat{\mathsf{q}}_{j\pm1/2} \circ \mathbf{F}_{j\pm1/2} \circ \hat{\mathsf{q}}_{j\pm1/2}^*$, with $\mathsf{R}_{j\pm1/2} = \mathfrak{E}(\hat{\mathsf{q}}_{j\pm1/2})$, as stated in (4). Making use of the identities $h_{j\pm1/2} \partial \mathbf{\Gamma}_{j\pm1/2}/\partial \mathbf{r}_j = \mp \mathsf{R}_{j\pm1/2}$, one finally obtains the difference term $\mathbf{f}_{j+1/2} - \mathbf{f}_{j-1/2} = -\partial \mathscr{W}^{(el)}/\partial \mathbf{r}_j$ according to the chain rule and the expressions discussed above.

Altogether, we arrive at the *semi-discrete linear momentum balance* equation in the desired form

$$\mathbf{f}_{j+1/2} - \mathbf{f}_{j-1/2} + \bar{h}_j \boldsymbol{\beta}_j = \frac{\partial \bar{\mathscr{L}}}{\partial \mathbf{r}_j} = \partial_t \left(\frac{\partial \bar{\mathscr{L}}}{\partial \mathbf{v}_j} \right) = \bar{h}_j \rho_j \partial_t \mathbf{v}_j \,, \tag{11}$$

as formulated in (2) according to a finite volume type approach, but here derived by Lagrangian mechanics. We wish to remark that the equation itself is identical to the one given in [2], and also its derivation more or less mimics the derivation given in that work for the special case of linear constitutive relations.

---

[2] In this work we are primarily interested to point out the relation of Lagrangian Cosserat rod mechanics to a discretization approach directly applied to the balance equations of the continuum model. Therefore, we omit the discussion of details related to the special form of the discrete equations near the boundaries. Also, our treatment of the quaternionic d.o.f. is kept at a formal level. For technical details related to the enforcement of unit norm constraints via Lagrangian multipliers and similar issues we refer to [2].

The derivation of the second system (3) of balance equations by the Lagrangian formalism is a more complicated task due to derivative operations w.r.t. *rotational* variables. The semi-discrete eqns. (3) do not result directly from Euler–Lagrange equations formulated in terms of the quaternion frames $\{\hat{q}_{j-1/2}\}_{j=1,\dots,N}$, but are obtained by taking *rotational gradients* [1] w.r.t. the directors $\mathbf{a}_{j-1/2}^{(k)} = R_{j-1/2} \cdot \mathbf{e}_k$ of the corresponding $SO(3)$ frames $R_{j-1/2} = \mathfrak{E}(\hat{q}_{j-1/2})$.

In the continuous theory, the external moment $\boldsymbol{\mu}$ was assumed to be derivable from a potential function $\mathscr{V}_{\boldsymbol{\mu}}^{(ext)}(R)$ depending on $R = \mathbf{a}^{(k)} \otimes \mathbf{e}_k$ according to $\boldsymbol{\mu} = -\nabla_R \mathscr{V}_{\boldsymbol{\mu}}^{(ext)} \equiv -\mathbf{a}^{(k)} \times \partial \mathscr{V}_{\boldsymbol{\mu}}^{(ext)}/\partial \mathbf{a}^{(k)}$. By analogous algebraic calculations one finds that $-\nabla_R \mathscr{V}_{\mathbf{F}}^{(el)}(\boldsymbol{\Gamma}) = \partial_s \mathbf{r} \times \mathbf{f}$ holds for the potential function $\mathscr{V}_{\mathbf{F}}^{(el)}$ of $\boldsymbol{\Gamma} = R^T \cdot \partial_s \mathbf{r} = \langle \mathbf{a}^{(k)}, \partial_s \mathbf{r} \rangle \mathbf{e}_k$ from which the spatial force vector $\mathbf{f} = R \cdot \partial \mathscr{V}_{\mathbf{F}}^{(el)}/\partial \boldsymbol{\Gamma}$ is obtained. Using the definitions (5) and (7) of the semi-discrete model, both expressions can be directly transferred to obtain their discrete counterparts as gradients of the respective potentials w.r.t. the frames $R_{j+1/2}$, according to: $-\nabla_{R_{j+1/2}} \mathscr{W}_{\boldsymbol{\mu}}^{(ext)} = -h_{j+1/2} \nabla_{R_{j+1/2}} \mathscr{V}_{\boldsymbol{\mu}}^{(ext)}(R_{j+1/2}) = h_{j+1/2} \boldsymbol{\mu}_{j+1/2}$ and $-\nabla_{R_{j+1/2}} \mathscr{W}_{\mathbf{F}}^{(el)} = -h_{j+1/2} \nabla_{R_{j+1/2}} \mathscr{V}_{\mathbf{F}}^{(el)}(\boldsymbol{\Gamma}_{j+1/2}) = (\mathbf{r}_{j+1} - \mathbf{r}_j) \times \mathbf{f}_{j+1/2}$, where $\mathbf{f}_{j+1/2} = R_{j+1/2} \cdot \partial \mathscr{V}_{\mathbf{F}}^{(el)}/\partial \boldsymbol{\Gamma}_{j+1/2}$.

Next, we consider the terms resulting from gradients of the discrete potential function $\mathscr{W}_{\mathbf{M}}^{(el)}$ defined in (6) w.r.t. the frame variables: As in terms of $SO(3)$ frames the discrete curvatures are given by $\mathbf{K}_j \simeq \tilde{\mathbf{K}}_j = \log(R_{j-1/2}^T \cdot R_{j+1/2})/\bar{h}_j$ with the usual identification of $\mathfrak{so}(3)$ mappings and vectors in $\mathbb{E}^3$, the frame $R_{j+1/2}$ appears only in the two terms of the sum (6) that depend on $\mathbf{K}_j$ and $\mathbf{K}_{j+1}$, such that $\nabla_{R_{j+1/2}} \mathscr{W}_{\mathbf{M}}^{(el)} = \bar{h}_j \nabla_{R_{j+1/2}} \mathscr{V}_{\mathbf{M}}^{(el)}(\mathbf{K}_j) + \bar{h}_{j+1} \nabla_{R_{j+1/2}} \mathscr{V}_{\mathbf{M}}^{(el)}(\mathbf{K}_{j+1})$. As stated in [7] for the quaternionic formulation, the material difference rotation $W_j := R_{j-1/2}^T \cdot R_{j+1/2}$ from which the discrete material curvatures $\mathbf{K}_j \simeq \tilde{\mathbf{K}}_j = \log(W_j)/\bar{h}_j$ are extracted may be rotated forward by *either* of the two adjacent frames $R_{j\pm1/2}$ with the identical result $w_j := R_{j\pm1/2} \cdot W_j \cdot R_{j\pm1/2}^T \equiv R_{j+1/2} \cdot R_{j-1/2}^T$. Therefore, the discrete *vertex based spatial curvatures* $\log(w_j)/\bar{h}_j \simeq \boldsymbol{\kappa}_j = R_{j\pm1/2} \cdot \mathbf{K}_j$ are well defined quantities. Using our definition of discrete curvatures $\mathbf{K}_j$, material moment vectors given by $\mathbf{M}_j = \partial \mathscr{V}_{\mathbf{M}}^{(el)}/\partial \mathbf{K}_j$ and spatial moment vectors defined as $\mathbf{m}_j := R_{j+1/2} \cdot \mathbf{M}_j$, one may derive the identities $\bar{h}_j \nabla_{R_{j+1/2}} \mathscr{V}_{\mathbf{M}}^{(el)}(\mathbf{K}_j) = \bar{h}_j \nabla_{R_{j+1/2}} \langle \mathbf{K}_j, \mathbf{M}_j \rangle = R_{j+1/2} \cdot \mathbf{M}_j = \mathbf{m}_j$ and $\bar{h}_{j+1} \nabla_{R_{j+1/2}} \mathscr{V}_{\mathbf{M}}^{(el)}(\mathbf{K}_{j+1}) = \bar{h}_{j+1} \nabla_{R_{j+1/2}} \langle \mathbf{K}_{j+1}, \mathbf{M}_{j+1} \rangle = -R_{j+3/2} \cdot \mathbf{M}_{j+1} = -\mathbf{m}_{j+1}$, adding up to $-\nabla_{R_{j+1/2}} \mathscr{W}_{\mathbf{M}}^{(el)} = \mathbf{m}_{j+1} - \mathbf{m}_j$ as desired. This outlines the derivation of the l.h.s. of the balance equation (3) in terms of gradients w.r.t. the $SO(3)$ frames as:

$$-\nabla_{R_{j+1/2}} \mathscr{W}^{(pot)} = -\nabla_{R_{j+1/2}} \left[\mathscr{W}^{(el)} + \hat{\mathscr{W}}^{(ext)} \right] = \mathbf{m}_{j+1} - \mathbf{m}_j + (\mathbf{r}_{j+1} - \mathbf{r}_j) \times \mathbf{f}_{j+1/2} + h_{j+1/2} \boldsymbol{\mu}_{j+1/2} . \qquad (12)$$

The inertial terms on the r.h.s. of (3) are obtained analogous to the derivation in the continuous theory in terms of the gradient operator $\nabla_{\partial_t R} \mathscr{T} := \mathbf{a}^{(k)} \times \partial \mathscr{T}/\partial(\partial_t \mathbf{a}^{(k)})$ w.r.t. the time derivative $\partial_t R = \partial_t \mathbf{a}^{(k)} \otimes \mathbf{e}_k$ of $SO(3)$ frames. Applied to $\mathscr{T} = \frac{1}{2} \rho_L \mathbf{v}^2 + \frac{1}{2} \langle \boldsymbol{\Omega}^T, [\rho I_0] \cdot \boldsymbol{\Omega} \rangle$ this results in $\nabla_{\partial_t R} \mathscr{T} = \nabla_{\partial_t R} \frac{1}{2} \langle \boldsymbol{\Omega}^T, [\rho I_0] \cdot \boldsymbol{\Omega} \rangle = [\rho_L J] \cdot \boldsymbol{\omega}$, with the spatial inertia tensor $[\rho_L J] = R \cdot [\rho I_0] \cdot R^T$ and the spatial angular velocity $\boldsymbol{\omega} = \frac{1}{2} \mathbf{a}^{(k)} \times \partial_t \mathbf{a}^{(k)} = R \cdot \boldsymbol{\Omega}$ of the moving frame, where $\boldsymbol{\Omega} \simeq \tilde{\Omega} = R^T \cdot \partial_t R$. For the discrete model, all algebraic computations can be applied to the rotational part (9) of the discrete kinetic energy function without modification, with the result

$$\nabla_{\partial_t R_{j+1/2}} \mathscr{W}^{(kin)} = \nabla_{\partial_t R_{j+1/2}} \mathscr{W}^{(rot)} = h_{j+1/2} [\rho_L J]_{j+1/2} \cdot \boldsymbol{\omega}_{j+1/2} , \qquad (13)$$

where the spatial inertia tensor $[\rho_L J]_{j+1/2} = R_{j+1/2} \cdot [\rho I_0]_{j+1/2} \cdot R_{j+1/2}^T$ and angular velocity $\boldsymbol{\omega}_{j+1/2} = R_{j+1/2} \cdot \boldsymbol{\Omega}_{j+1/2}$ of each edge segment of the discrete Cosserat rod are defined in complete analogy to the continuous theory. Note that due to $\partial_t([\rho_L J] \cdot \boldsymbol{\omega}) = [\rho_L J] \cdot \partial_t \boldsymbol{\omega} + \boldsymbol{\omega} \times [\rho_L J] \cdot \boldsymbol{\omega}$ the time derivative of r.h.s. of (13) already contains a part equal to the contribution of the term $-\nabla_{R_{j+1/2}} \mathscr{W}^{(rot)} = h_{j+1/2} \boldsymbol{\omega}_{j+1/2} \times [\rho_L J]_{j+1/2} \cdot \boldsymbol{\omega}_{j+1/2}$.

In summary, these considerations indicate how the *semi-discrete angular momentum balance* equation

$$\mathbf{m}_{j+1} - \mathbf{m}_j + (\mathbf{r}_{j+1} - \mathbf{r}_j) \times \mathbf{f}_{j+1/2} + h_{j+1/2} \boldsymbol{\mu}_{j+1/2} = h_{j+1/2} \partial_t \left([\rho_L J]_{j+1/2} \cdot \boldsymbol{\omega}_{j+1/2} \right) \qquad (14)$$

results by computing both sides of the equivalent equation $-\nabla_{R_{j+1/2}} \mathscr{W}^{(pot)} = \partial_t(\nabla_{\partial_t R_{j+1/2}} \mathscr{W}^{(kin)})$ formulated in terms of variational derivatives w.r.t. the edge based $SO(3)$ frames according to the Lagrangian formalism.

A *quaternionic* formulation of the *rotational gradient operators* ∇_R and $\nabla_{\partial_t R}$ provides the connection to the Euler–Lagrange equations of the quaternionic formulation: The parametrization $R = \mathfrak{E}(\hat{q})$ of $SO(3)$ frames by rotational quaternions via the Euler map and the representation $\mathbf{a}^{(k)} = \mathfrak{E}(\hat{q}) \cdot \mathbf{e}_k$ of frame directors imply the transformation rule $\partial/\partial \mathbf{a}^{(k)} = [d\mathfrak{E}(\hat{q}) \cdot \mathbf{e}_k]^{-T} \cdot \partial/\partial \hat{q}$ of the gradients w.r.t. the frame directors and the *quaternion gradient*[3] operator $\partial/\partial \hat{q}$.

---

[3]Note that for a scalar function $\mathscr{V}(\hat{q})$ of $\hat{q} \in S^3$ the vector $\partial \mathscr{V}/\partial \hat{q}$ is orthogonal to $\hat{q}$, i.e.: $\langle \hat{q}, \partial \mathscr{V}/\partial \hat{q} \rangle \equiv 0$.

Utilizing the *dot truncation rule* [11] one finds that likewise $\partial/\partial(\partial_t\mathbf{a}^{(k)}) = [\mathrm{d}\mathfrak{E}(\hat{\mathsf{q}})\cdot\mathbf{e}_k]^{-T}\cdot\partial/\partial(\partial_t\hat{\mathsf{q}})$ holds for the transformation of the gradients w.r.t. the frame director velocities. Therefore, the *quaternionic* rotational gradient operators are given by $\nabla_{\mathsf{R}} \equiv \nabla_{\hat{\mathsf{q}}} := (\mathfrak{E}(\hat{\mathsf{q}})\cdot\mathbf{e}_k)\times[\mathrm{d}\mathfrak{E}(\hat{\mathsf{q}})\cdot\mathbf{e}_k]^{-T}\cdot\partial/\partial\hat{\mathsf{q}}$ and $\nabla_{\partial_t\mathsf{R}} \equiv \nabla_{\partial_t\hat{\mathsf{q}}} := (\mathfrak{E}(\hat{\mathsf{q}})\cdot\mathbf{e}_k)\times[\mathrm{d}\mathfrak{E}(\hat{\mathsf{q}})\cdot\mathbf{e}_k]^{-T}\cdot\partial/\partial(\partial_t\hat{\mathsf{q}})$, where $\mathbf{p}\times\mathbf{q} = \frac{1}{2}(\mathbf{p}\circ\mathbf{q} - \mathbf{q}\circ\mathbf{p})$ abbreviates the quaternionic formulation of the cross product of vectors in $\mathbb{E}^3$, and the semi-discrete balance equations (14) may likewise be obtained from $-\nabla_{\hat{\mathsf{q}}_{j+1/2}}\mathscr{W}^{(pot)} = \partial_t(\nabla_{\partial_t\hat{\mathsf{q}}_{j+1/2}}\mathscr{W}^{(kin)})$, using the discrete energy terms $\mathscr{W}^{(pot)}$ and $\mathscr{W}^{(kin)}$ expressed in quaternion variables.

It remains to show that the equations $-\nabla_{\hat{\mathsf{q}}}\mathscr{W}^{(pot)} = \partial_t(\nabla_{\partial_t\hat{\mathsf{q}}}\mathscr{W}^{(kin)})$ may be rewritten as $(\mathfrak{E}(\hat{\mathsf{q}})\cdot\mathbf{e}_k)\times[\mathrm{d}\mathfrak{E}(\hat{\mathsf{q}})\cdot\mathbf{e}_k]^{-T}\cdot[\partial\bar{\mathscr{L}}/\partial(\hat{\mathsf{q}}) - \partial_t(\partial\bar{\mathscr{L}}/\partial(\partial_t\hat{\mathsf{q}}))] = \mathbf{0}$, which in turn implies that, due to the regularity of the transformation operator $(\mathfrak{E}(\hat{\mathsf{q}})\cdot\mathbf{e}_k)\times[\mathrm{d}\mathfrak{E}(\hat{\mathsf{q}})\cdot\mathbf{e}_k]^{-T}$, the rotational part of the Euler–Lagrange equations (10) and the balance equations (14) are indeed equivalent. However, a presentation of the technically involved derivation of this statement is beyond the scope of (or rather: available space for) this conference paper. The derivation presented in [2] aims at (and results in) a quaternionic version of angular momentum balance that is primarily useful for *numerical* computations. Different from that, the derivation presented in this section aims at pointing out the formal similarity of the semi-discrete and continuous balance equations, in accordance with the Lagrangian formalism.

3. Static equilibria obtained by energy minimization

Hamilton's principle characterizes static equilibrium configurations as stationary points of the potential energy, and stable ones as minima of the latter. Therefore the static balance equations

$$\mathbf{f}_{j+1/2} - \mathbf{f}_{j-1/2} + \bar{h}_j\boldsymbol{\beta}_j = \mathbf{0} \quad\Leftrightarrow\quad \partial\mathscr{W}^{(pot)}/\partial\mathbf{r}_j = \mathbf{0} \tag{15}$$

$$\mathbf{m}_{j+1} - \mathbf{m}_j + (\mathbf{r}_{j+1} - \mathbf{r}_j)\times\mathbf{f}_{j+1/2} + h_{j+1/2}\boldsymbol{\mu}_{j+1/2} = \mathbf{0} \quad\Leftrightarrow\quad \partial\mathscr{W}^{(pot)}/\partial\hat{\mathsf{q}}_{j+1/2} = \mathbf{0} \tag{16}$$

hold for stable equilibrium configurations corresponding to minima of the potential energy $\mathscr{W}^{(pot)}$. To illustrate the properties of our discrete rod model, we briefly discuss two well-known academic examples[4]:

(a) *Plane deformations of an elastic band* (e.g. a leaf spring), clamped on one end and loaded by a force on the other one, can be modeled analytically using *Euler's Elastica* theory [13, 14].

(b) *Helical deformations of a flexible rod* (e.g. a steel string or a glass fiber) *in space* are an elementary application of the rod theory of Kirchhoff and Clebsch [15, 16].

For both examples, we assume that there are no external forces or moments acting on the rod (i.e. $\boldsymbol{\beta} = \mathbf{0} = \boldsymbol{\mu}$), such that the sectional force $\mathbf{f}$ is constant, and it remains to solve $\partial_s\mathbf{m} + \partial_s\mathbf{r}\times\mathbf{f} = \mathbf{0}$ for given boundary conditions. Note that in equilibrium the spatial moment quantity $\mathfrak{M} := \mathbf{m}(s) + \mathbf{r}(s)\times\mathbf{f}$ is necessarily *constant along the rod* for constant $\mathbf{f}$, independent of its constitutive properties. For the discrete rod model, minimization of its energy implies constant $\mathbf{f}_{j-1/2} \equiv \mathbf{f}$ on all edges, and the discrete balance equations $\mathbf{m}_j - \mathbf{m}_{j-1} = \mathbf{f}\times(\mathbf{r}_j - \mathbf{r}_{j-1})$ satisfied by minimal energy configurations, such that $\mathfrak{M}_j = \mathbf{m}_j + \mathbf{r}_j\times\mathbf{f}$ is constant on all vertices.

Both examples can be treated analytically using an *inextensible Kirchhoff rod* model, for which any length changes of the centerline as well as transverse shearing of the frames are kinematically inhibited. Differently, our discrete Cosserat model allows for tangential extension or compression of the discrete centerline as well as transverse shearing of the frames w.r.t. the edge tangents. However, for load cases primarily characterized by bending and twisting, these deformations are negligibly small. Nevertheless, they are present and provide the discrete strains used to evaluate the discrete sectional forces $\mathbf{f}_{j-1/2} = \hat{\mathsf{q}}_{j-1/2}\circ\mathbf{F}_{j-1/2}\circ\hat{\mathsf{q}}^*_{j-1/2}$ from the constitutive equations $\mathbf{F}_{j-1/2} = \mathsf{C}_\Gamma\cdot(\boldsymbol{\Gamma}_{j-1/2} - \mathbf{e}_3)$ on all edges. Discrete material moments are computed on vertices as $\mathbf{M}_j = \mathsf{C}_K\cdot(\mathbf{K}_j - \mathbf{K}_{0j})$, where $\mathbf{K}_{0j} \equiv \mathbf{0}$ for both examples. Spatial moments $\mathbf{m}_j = \hat{\mathsf{q}}_{j\pm1/2}\circ\mathbf{M}_j\circ\hat{\mathsf{q}}^*_{j\pm1/2}$ are obtained by rotation of the material ones, using either of the adjacent frames involved in the computation of the discrete material curvature $\mathbf{K}_j$.

Example (a) Euler's Elastica: The deformed rod configurations shown in Figs. 2 and 3 result from two very different solution approaches: Modeling the rod as a plane, inextensible elastic curve with a centerline $\mathbf{r}(s) = \int_0^s d\zeta\,\mathbf{t}(\zeta)$ obtained by integration of its unit tangent vector $\mathbf{t}(s) = \cos(\theta(s))\mathbf{e}_1 + \sin(\theta(s))\mathbf{e}_2$ reduces the static equilibrium equations to a nonlinear boundary value problem (BVP) for the tangent angle $\theta(s)$ as a function of the arc length, which can be solved analytically in closed form. The other equilibrium configurations shown in Figs. 2 and 3 are obtained via energy minimization of a discrete Cosserat rod in space.

---

[4]We refer to Ch. XIX, Art. 260-263 and 270 Love's treatise [12] for a concise discussion of an analytical treatment of both examples.
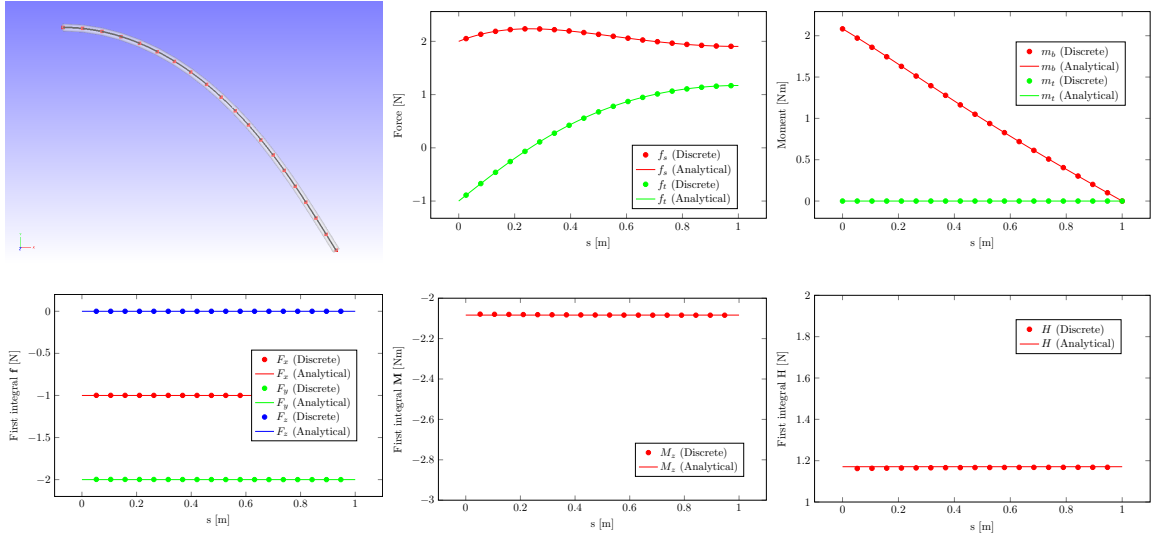
Figure 2: Visual and quantitative comparison of the discrete Cosserat rod model (20 vertices) in static equilibrium and the analytical solution of an *Elastica* of reference length $L = 1000$ mm and bending stiffness $[EI] = 1.0$ Nm^2, evaluated in *Matlab* for the load force $\mathbf{f}_L = -2\mathbf{e}_1 - 1\mathbf{e}_2$ N (add. Cosserat rod parameters: $[GA] = 10.0$ kN $= [EA]/3$).
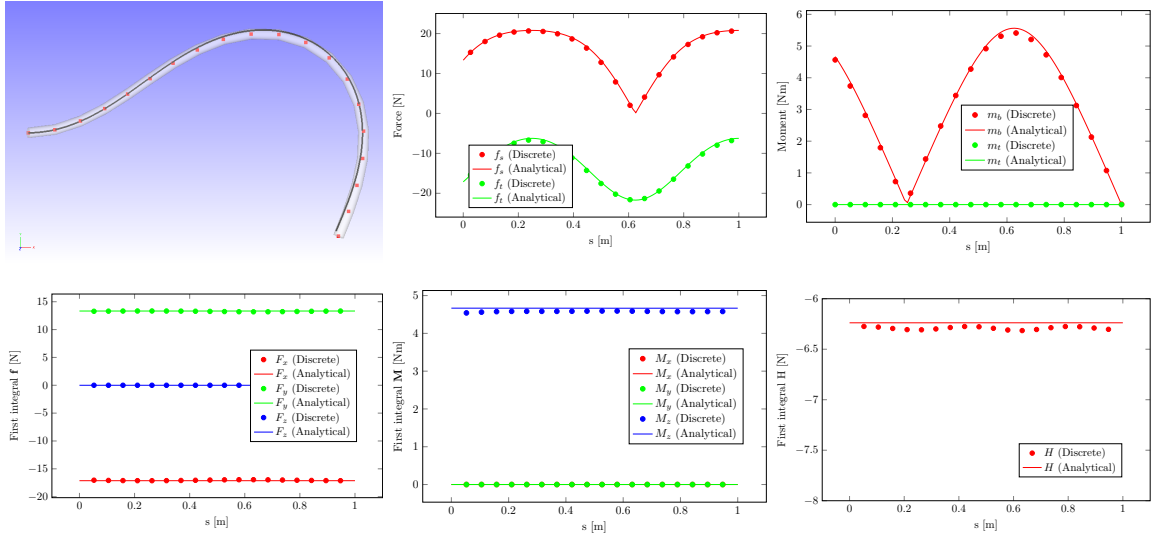

Figure 3: Visual and quantitative comparison of the discrete Cosserat rod model (20 vertices) in static equilibrium and the analytical solution of an *Elastica* of reference length $L = 1000$ mm and bending stiffness $[EI] = 1.0$ Nm^2, evaluated in *Matlab* for the load forces $\mathbf{f}_L = -17.8\mathbf{e}_1 + 12.8\mathbf{e}_2$ N (add. Cosserat rod parameters: $[GA] = 10.0$ kN $= [EA]/3$).

The boundary condition at the clamped end is $\theta(0) = 0$, at the other end the rod is loaded by a force $-\mathbf{f}_L = f_1\mathbf{e}_1 + f_2\mathbf{e}_2 = \mathbf{f}(L)$. As $\mathbf{f}(s) \equiv -\mathbf{f}_L$ remains constant along the rod, the balance equation for $\mathbf{m}_b = [EI]\mathbf{t} \times \partial_s\mathbf{t} = EI\theta'(s)\mathbf{e}_3$ reduces to the differential equation $[EI]\theta''(s) = f_1\sin(\theta(s)) - f_2\cos(\theta(s))$ for the tangent angle. The bending moment $\mathbf{m}_b$ and likewise the (signed) the curvature $\kappa(s) = \theta'(s)$ vanish at the loaded end, which provides the additional boundary condition $\theta'(L) = 0$. For given length L and bending stiffness $[EI]$ of the *Elastica* and given end force $\mathbf{f}_L$, the two–point BVP for $\theta(s)$ can be solved analytically in closed form in terms of Jacobian elliptic functions.

The constancy of the function $H = \frac{1}{2}\mathbf{m}_b^2/[EI] + \langle \mathbf{f}, \mathbf{t} \rangle = \frac{1}{2}[EI]\theta'(s)^2 + f_1\cos(\theta(s)) + f_2\sin(\theta(s))$ along the *Elastica* solution can be utilized to integrate the DE for $\theta(s)$ by a separation of variables. For an *Elastica* confined to the plane spanned by $\{\mathbf{e}_1, \mathbf{e}_2\}$ only the third component $\mathfrak{M}_3 = [EI]\kappa(s) + f_2 x(s) - f_1 y(s)$ of the first integral $\mathfrak{M}$ may take a nonzero constant value along the the centerline curve $\mathbf{r}(s) = x(s)\mathbf{e}_1 + y(s)\mathbf{e}_2$ in equilibrium. Due to the boundary conditions $\mathbf{r}(0) = \mathbf{0}$, $\mathbf{m}_b(L) = \mathbf{0}$ and $\mathbf{f}(L) = -\mathbf{f}_L$ the relation $[EI]\kappa(0) = f_1 y_L - f_2 x_L$ holds for the bending moment at the clamped end and the sectional force at the end position $\mathbf{r}(L) = x_L\mathbf{e}_1 + y_L\mathbf{e}_2$ of the *Elastica*.

Equilibrium solutions of the discrete Cosserat rod are computed by minimizing its elastic energy for given boundary conditions by an interior point method, using the software package IPOPT. To compute solutions for the plane *Elastica* problem, the discrete model is *not* a priori confined to plane. Nevertheless, discrete centerline curves with all vertices $\{\mathbf{r}_j\}_{j=0,\ldots,N}$ located in the plane of the problem result from the numerical solution. Although closed form analytical solutions of the equivalent two–point BVP for the tangent angle $\theta(s)$ of the *Elastica* in principle could be obtained in terms of special functions, we computed *numerical solutions* of the BVP for $\theta(s)$ with the *Matlab* routine bvp4c, using a very fine discretization to approximate the analytical *Elastica* solution with high precision, to circumvent technical problems encountered in the vicinity of inflection points. Typical application cases treated in *IPS* imply the specification of kinematical boundary conditions (i.e. the prescription of centerline positions, frames, or both) at the ends of a cable, rather than the prescription of loads. Correspondingly, in the shown example we clamped the position and frame of the rod at the left end, and prescribed the position of its other end. The sectional force $\mathbf{f}_L$ was then extracted from the *IPS* solution in post processing and used as an input for the integration of the *Elastica* BVP in *Matlab*.

The screenshots displayed in Figs. 2 and 3 show the numerical solutions obtained for our discrete Cosserat rod model, visualized in the GUI of the *IPS*[5] software, with the vertices indicated by red dots, and an overlay of the *Elastica* curve obtained from *Matlab* for the two cases. For the *Elastica* solution, the plotted quantities display the values of the tangential force component $f_t(s) = \langle \mathbf{f}, \mathbf{t}(s) \rangle$, the norm $f_s(s) = \|\mathbf{f} - \langle \mathbf{f}, \mathbf{t}(s) \rangle \mathbf{t}(s)\|$ of the shear force, the norm $m_b = [EI]\sqrt{\kappa^2(s)}$ of the bending moment as well as the values of the first integrals $\mathbf{f}$, $\mathfrak{M}$ and H along the centerline. For completeness, also the torsional moment m_t is displayed, which for the plane *Elastica* problem vanishes identically, by definition for the analytical solution, and for the discrete rod as a result of the numerical computations.

For the equilibrium solution of the discrete Cosserat rod model obtained by energy minimization, the values of discrete curvature κ_j and therefore also those of the bending moment $m_{bj} = [EI]\sqrt{\kappa_j^2}$ are defined at the vertex positions $\mathbf{r}_j$ of the discrete centerline, while the sectional forces $\mathbf{f}_{j-1/2}$ are obtained from the discrete shear strains $\mathbf{\Gamma}_{j-1/2}$ on edges and need to be interpolated as weighted averages $\bar{\mathbf{f}}_j := (h_{j-1/2}\mathbf{f}_{j-1/2} + h_{j+1/2}\mathbf{f}_{j+1/2})/(2\bar{h}_j)$ to obtain vertex based sectional forces, which in turn may be used to define a discrete vertex based approximation $\bar{\bar{\mathfrak{M}}}_j = \mathbf{m}_j + \mathbf{r}_j \times \bar{\mathbf{f}}_j$ of the conserved total moment $\mathfrak{M}$. A discrete approximation $\bar{H}_j \approx H(s_j)$ of the first integral H needs to be constructed in a similar manner, taking into account that for the Cosserat rod model the extensional force components $F_{j-1/2}^{(3)} = \langle \mathbf{F}_{j-1/2}, \mathbf{e}_3 \rangle = \langle \mathbf{f}_{j-1/2}, \mathbf{a}_{j-1/2}^{(3)} \rangle$ replace the tangential force values $\langle \mathbf{f}_{j-1/2}, \mathbf{t}_{j-1/2} \rangle$ generally used in the definition of H for inextensible Kirchhoff rods. Likewise, the elastic energy term of the inextensible *Elastica* needs to be replaced by the more general stored energy density of a Cosserat rod (see [20] for details). While the term $\mathscr{V}_{\mathbf{M}}^{(el)}(\mathbf{K}_j)$ is by definition evaluated at vertices, the terms $\mathscr{V}_{\mathbf{F}}^{(el)}(\mathbf{\Gamma}_{j\pm1/2})$ as well as $\langle \mathbf{F}_{j\pm1/2}, \mathbf{e}_3 \rangle$ are edge based and require an interpolation to compute an approximation of their vertex based values. This is done by the same weighted averaging scheme as used to obtain $\bar{\mathbf{f}}_j$.

For the moderate, cantilever-type deformations shown in Fig. 2 the numerical solution obtained for the discrete Cosserat rod by energy minimization agrees almost perfectly with the analytical *Elastica* solution in all aspects.

For the more demanding test case shown in Fig. 3 one still obtains good, but not as perfect agreement, as there are small, but clearly visible differences between the centerlines of the discrete model and the *Elastica*. On the one hand, the discrete force vectors $\bar{\mathbf{f}}_j$ are accurately conserved, and also the tangential and shear force components and the bending moment closely follow the analytical curves[6]. However, the small deviations of the non-zero component $\mathfrak{M}_j^{(3)}$ from a constant value (which must not necessarily equal the one of the continuous model) indicates that the discrete configuration is not in perfect equilibrium. This is presumably caused by the choice of algorithmic parameters of the numerical solution procedure, which seems to terminate too early in the case of more demanding deformation cases where the equilibrium is harder to find. As the function H is only constant in exact equilibrium, it is therefore not surprising that for $\bar{H}_j$ one recognizes corresponding small deviations from a constant value, and also slight deviations from the constant analytic value of H for the *Elastica* in equilibrium.

Nevertheless, the discussion of the results for the two examples shown in Figs. 2 and 3 demonstrates that the discrete Cosserat rod model combined with the approach to compute equilibrium solutions by energy minimization yields good results for the configuration variables as well as for the sectional kinetic quantities.

---

[5]The geometrically exact rod model currently used in the commercial version of *IPS Cable Simulation* is actually of *extensible Kirchhoff* type [17]. Corresponding benchmark tests like the ones displayed in the extended abstract submitted for this contribution had been performed in early development phases of the *IPS* software more than a decade ago. The main purpose of our present work is a thorough exploration of the *quasi-static* properties of the discrete Cosserat rod model [2] that was primarily developed for fully dynamic simulations.

[6]Note that for both the shear force and the bending moment their (non-negative) *absolute* values are plotted, which explains the sharp kinks in the respective curves at points where the signed quantities have roots with a change of sign. In the case of the shear force this happens when the force and tangent vectors are parallel, for the bending moment at points of inflection, where the tangent direction changes from a left to a right turn and the curvature becomes zero.
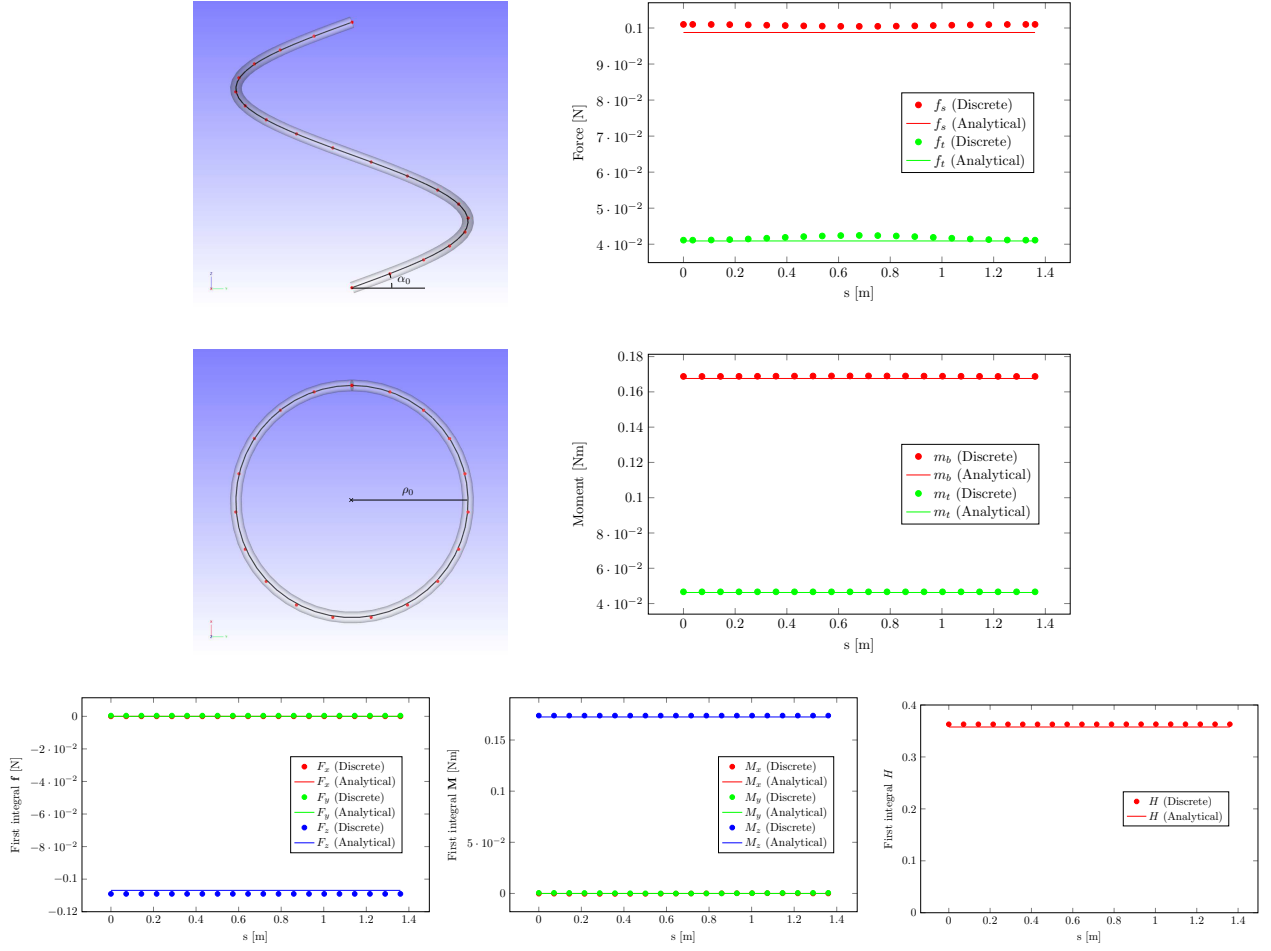
Figure 4: Visual and quantitative comparison of the discrete Cosserat rod model (20 vertices) in static equilibrium and Kirchhoff's analytical solution for a helix with bending / torsional stiffness $[EI] = 1.0 \, \text{Nm}^2 = [GJ]$, pitch angle $\alpha_0 = \pi/8$, radius $\rho_0 = 200$ mm and reference length $L = 2\pi\rho_0/\cos(\alpha_0) \approx 1360$ mm for one helical revolution (add. Cosserat rod parameters: $[GA] = 10.0$ kN $= [EA]/3$).

Example (b) Kirchhoff's helix: Helical deformations of a straight elastic rod in space can be treated analytically in closed form if modeled as an inextensible Kirchhoff rod (see [15] and [12] Art. 270).

The constitutive equation for the moment of the rod are given in spatial form as $\mathbf{m} = [EI]\, \mathbf{t} \times \partial_s \mathbf{t} + [GJ]\, \kappa^{(3)}\, \mathbf{t}$, where $\mathbf{t} \times \partial_s \mathbf{t} = \varkappa \mathbf{b}$ is the *curvature binormal* of the centerline with Frenet curvature $\varkappa = \sqrt{\kappa^{(1)} + \kappa^{(2)}}$, and $\kappa^{(3)}$ is the twist of the moving frame, such that $m_b = [EI]\, \varkappa$ is the absolute value of the bending moment around the binormal axis $\mathbf{b}$, and the value of the torsional moment directed (anti)parallel to $\mathbf{t}$ is the signed quantity $m_t = [GJ]\, \kappa^{(3)}$. Both m_t and the function $H = \frac{1}{2}[EI]\, \varkappa^2 + \frac{1}{2}[GJ]\, (\kappa^{(3)})^2 + \langle \mathbf{f}, \mathbf{t} \rangle$ are conserved along the centerline of an inextensible Kirchhoff rod deformed in space.

Helical configurations[7] are characterized by constant material curvature $\mathbf{K} = \kappa^{(k)}\, \mathbf{e}_k$ and may be held in equilibrium for specific combinations of the force and moment vectors, with $m_b = [EI]\, \cos^2(\alpha_0)/\rho_0$ and a resultant force value $F = [GJ]\, \kappa^{(3)} \cos(\alpha_0)/\rho_0 - [EI]\, \sin(\alpha_0) \cos^2(\alpha_0)/\rho_0^2$, where the axis of the helix is (anti)parallel to the force direction. In the example shown in Fig. 4 the helical axis is parallel to $\mathbf{e}_3$. The constant force $\mathbf{f} = F\mathbf{e}_3$ can be decomposed into its tangential and shear parts as $\mathbf{f} = F\left[\sin(\alpha_0)\, \mathbf{t} + \cos(\alpha_0)\, \mathbf{b}\right] = f_t\, \mathbf{t} + f_s\, \mathbf{b}$.

The screenshots displayed in in Fig. 4 show the side and top view of the discrete solution (vertices again indicated with red dots), with an overlay of the analytical helical centerline curve. As in the Elastica example, the forces, moments and first integrals show good agreement with their constant counterparts for the analytical solution.

---

[7] Helical equilibrium configurations exist also for uniform Cosserat rods [18, 19, 20] and are characterized by constant values of $\mathbf{K}$ and $\boldsymbol{\Gamma}$.

4. IPS Cable Simulation: Application examples from automotive industry

In automotive industry today, simulation tools are used in the realization of a new product. As changes in the design and planning concepts are extremely costly in later verification and production phases of the development process, much can be gained if a product design can be optimized and verified with respect to the assembly process with simulation tools as early as possible. Specifically, this holds true for the virtual preparation of slender flexible structures such as as electrical cables and wiring harnesses, hoses, pipes and tubes. In a complex product, these types of structures appear in a variety of applications, e.g. wired data communication, energy transfer (electrical power supply and hydraulics), heating and cooling systems, et cetera. They are usually located where there is restricted design space and are therefore often associated with quality problems and late on-line adjustments due to geometrical interference. Hence, there is a strong motivation to use a discrete simulation model to accurately predict deformations and stress in slender flexible structures already in the design phase ([21]).

Cosserat rods are particularly well suited for modeling of slender flexible structures encountered in industrial scenarios. The rod model accounts for large deformations and captures the interaction between the different deformation modes. At the same time, it is very efficient to evaluate, which is important when conducting iterative design studies, motion analysis and real-time manipulation. However, for industrial applications the rod model needs to be extended with additional functionality in order to be practical.

- **Pre-deformation:** This is a common property in e.g. plastic pipes and rubber hoses in order to keep the component in a chosen configuration implied by its geometrical design. A Cosserat rod model provides direct support to account for pre-deformation in terms of reference strains given by values of the invariants that are either prescribed or extracted from a desired nominal shape.

- **Systems of rod models:** A variety of different boundary conditions needs to be supported in order to model rods that are kinematically connected to each other and/or to other parts. Systems of cables and hoses typically involve (free-hanging) branching or break-out points. These boundary conditions can be included as constraints to the energy minimization problem when solving for static equilibrium, or they can enter as constraints (together with corresponding Lagrange multipliers) to the system of Euler–Lagrange equations when performing a dynamic simulation.

- **Mechanical clips:** Cables and hoses are oftentimes connected to each other or to rigid parts via mechanical clips with various allowed kinematic degrees of freedom. A typical clip can be modeled as a kinematic chain mechanism and is then added to the set of boundary conditions when connected to a rod model. The kinematic degrees of freedom are added as generalized variables in the system.

- **Contact handling:** Frictionless contact interaction between rods and between rods and triangulated surroundings needs to be treated as well. A huge computational bottleneck are the calculations of distance and collision with respect to the surrounding geometry that can potentially consist of millions of triangles.

Functionality as sketched in the list above, as well as a variety of additional productivity features, is implemented and supported in the simulation software *IPS Cable Simulation*. With the functionality in place, different case studies can be performed.

We illustrate this by a case study from the automotive industry depicted in Fig. 6. As the industry is focusing on electrified and hybrid solutions, both conventional combustion engines and battery supplied electrical engines need to fit in an already densely packed engine compartment. The lack of available design space makes it difficult to make qualified geometrical design decisions. The shown example is a static design study of three cooler hoses joined in a T-section connecting the radiator with the oil cooler and the engine cooling system. All three hoses are of rubber
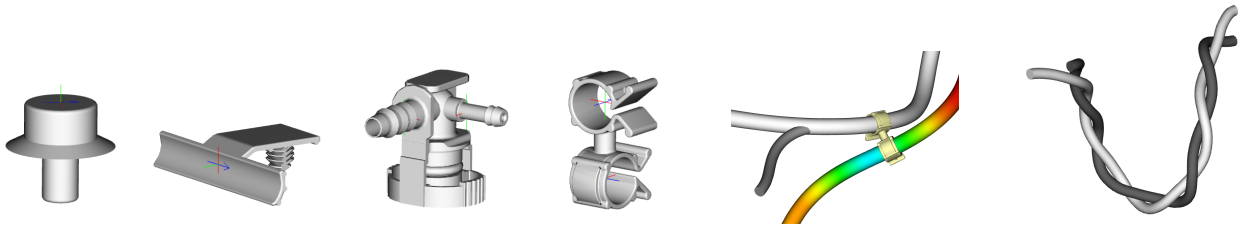

Figure 5: Examples of mechanical clips, an interconnected system of rods and contact handling between two rod models captured in the simulation software IPS Cable Simulation.
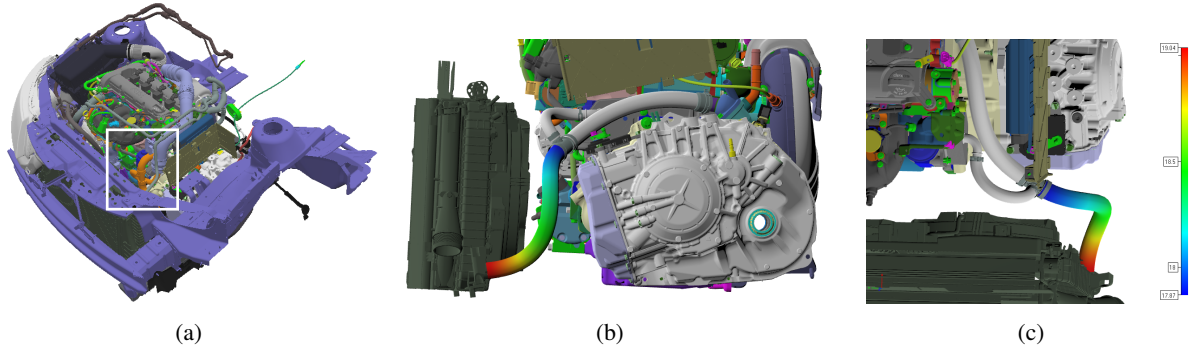
Figure 6: The industrial scenario. (a): The engine compartment of a car with the highlighted cooler hoses. (b) and (c): Side and top view of the static cooler hose case. Hose 1 is color-coded with internal force magnitude.
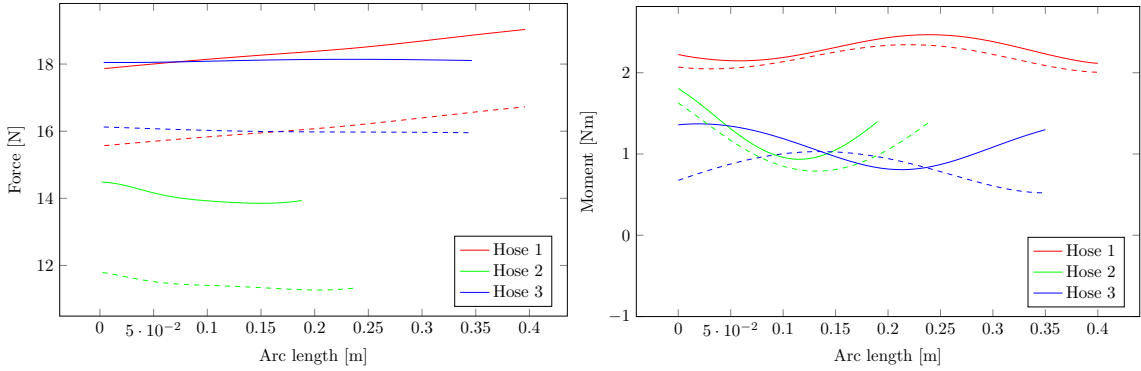

Figure 7: Distribution of internal force and moment in the three cooler hoses before (solid lines) and after (dashed lines) increasing the reference length of hose 2. The arc length parameter is measured from the junction.

material (Young's modulus $E = 5$ MPa, poisson ratio $v = 1/2$ and volume density $\rho = 1100$ kg/m^3). The inner / outer radius is 14.4 mm / 18.4 mm for hose 1 and 3 and 9.4 mm / 12.9 mm for hose 2. The reference arc lengths are 400 mm, 190 mm and 350 mm for hose 1, 2 and 3 respectively. The hoses are connected via a free-hanging rigid T-junction of mass 1 kg.

The distribution of internal forces and moments in the three hoses in static equilibrium is plotted in Fig. 7. It can be noted that the internal force in the smaller hose 2 is comparably high. By adding an extra design length of 50 mm to hose 2, the internal forces in all hoses have decreased significantly after the design change, whereas the internal moment remains roughly unaffected. In this way, design engineers can iteratively evaluate and modify the design of the product.

5. Conclusions

The present work investigates kinetic aspects of discrete quaternionic Cosserat rods defined on a staggered grid within the framework of Lagrangian mechanics. Theoretical considerations outline the main parts of a derivation of the semi-discrete spatial balance equations for linear and angular momentum via variational derivatives of the energy terms of the Lagrangian function of the rod model. Computing consecutive numerical solutions of the discrete quasi-static balance equations by sequential energy minimization provides a procedure that displays many favourable properties w.r.t. stability, robustness and computational performance. Besides its usefulness in automotive applications like interactive cable assembly simulations or the layout of cooler hoses in engine compartments, the discrete rod model combined with the energy minimization approach yields reliable results for the sectional forces and moments. Integrated into a software package like *IPS Cable Simulation*, this may be utilized by engineers to optimize their system layouts.

Acknowledgments

References

[1] P. Jung, S. Leyendecker, J. Linn and M. Ortiz: "A discrete mechanics approach to the Cosserat rod theory – Part 1: Static equilibria", *Int. J. Numer. Methods Eng.*, vol. 85, no. 1, pp. 31–60, 2011.

[2] H. Lang, J. Linn and M. Arnold: "Multibody dynamics simulation of geometrically exact Cosserat Rods", *Multibody System Dynamics*, vol. 25, no. 3, pp. 285–312, 2011.

[3] S.S. Antman: Nonlinear Problems of Elasticity, Springer, 2005.

[4] E. Reissner: "On one-dimensional large-displacement finite-strain beam theory", *Stud. Appl. Math.* vol. 52, no. 2, pp. 87–95, 1973.

[5] J.C. Simo: "A finite strain beam formulation: the three dimensional dynamic problem – Part I", *Comput. Meth. Appl. Mech. Eng.*, vol. 49, no. 1, pp. 55–70, 1985.

[6] M. Bergou, M. Wardetzky, S. Robinson, B. Audoly and E. Grinspun: "Discrete Elastic Rods", *ACM Transaction on Graphics (SIGGRAPH)*, vol. 27, no. 3, pp. 63:1–63:12, 2008.

[7] J. Linn: "Discrete kinematics of Cosserat rods based on the difference geometry of framed curves", *Proceedings of the 4th Joint International Conference on Multibody System Dynamics IMSD 2016*, Montréal, 2016.

[8] S.L. Han and O.A. Bauchau: "Nonlinear Three-Dimensional Beam Theory for Flexible Multibody Dynamics", *Multibody System Dynamics*, vol. 34, no. 3, pp. 211–242, 2015.

[9] J. Linn, H. Lang and A. Tuganov: "Geometrically exact Cosserat rods with Kelvin–Voigt type viscous damping", *Mechanical Sciences*, vol. 4, pp. 79–96, 2013.

[10] J. Linn and K. Dreßler: "Discrete Cosserat rod models based on the difference geometry of framed curves for interactive simulation of flexible cables", to be published in L. Ghezzi, D. Hömberg and C. Landry (Eds.): *Math for the Digital Factory*, Springer, 2017.

[11] H. Lang and J. Linn: "Lagrangian field theory in space and time for geometrically exact Cosserat rods", *Reports of the ITWM*, Nr. 150, 2009.

[12] A.E.H. Love: A Treatise on the Mathematical Theory of Elasticity (4th ed.), Cambridge University Press, 1927.

[13] L. Euler: Addimentatum I de curvis elasticis, p. 247 ff. in *Methodus inveniendi lineas curvas maximi minimive proprietate gaudentes, sive solutio problematis isoperimetrici lattissimo sensu accepti*, *Opera Omnia I*, vol. 24, pp. 231–297, Bousquent, Lausanne, 1744.

[14] C. Truesdell: Euler's treatise on elastic curves (1743). I. Static deflection, Part II, sec. 28, p. 219 ff. in *The Rational Mechanics of Flexible or Elastic Bodies 1638–1788. Introduction to Leonardi Euleri Opera Omnia Vol. X et XI seriei secundae*, Füssli, 1960.

[15] G. Kirchhoff: "Über das Gleichgewicht und die Bewegung eines unendlich dünnen elastischen Stabes", pp. 285–316 in *Gesammelte Abhandlungen*, Johann Ambrosius Bart, Leipzig, 1882.

[16] H.E. Dill: "Kirchhoff's Theory of Rods", *Arch. Hist. Exact Sciences*, vol. 44, no. 1, pp. 1–23, 1992.

[17] J. Linn, T. Stephan, J. Carlsson and R. Bohlin: "Fast Simulation of Quasistatic Rod Deformations for VR Applications", L.L. Bonilla, M. Moscoso, G. Platero and J.M. Vega (Eds.): *Progress in Industrial Mathematics at ECMI 2006*, pp. 247–253, Springer, 2008.

[18] S.S. Antman: "Kirchhoff's problem for nonlinearly elastic rods", *Quart. Appl. Math.*, vol. 32, pp. 221–240, 1974.

[19] A.B. Whitman and C.N. DeSilva: "An exact solution in a nonlinear theory of rods", *Journal of Elasticity*, vol. 4, no. 4, pp. 265–280, 1974.

[20] N. Chouaieb and J.H. Maddocks: "Kirchhoff's Problem of Helical Equilibria of Uniform Rods", *Journal of Elasticity*, vol. 77, pp. 221–247, 2004.

[21] T. Hermansson: Computational Methods for Deformable 1D Objects in Virtual Product Realization, Thesis for the degree of Licentiate of Engineering, ISSN: 1652–9243, Göteborg, 2017.